Published online 21 July 2017

Nucleic Acids Research, 2017, Vol. 45, No. 16 ***9547–9557***
doi: 10.1093/nar/gkx638

Number of inadvertent RNA targets for morpholino knockdown in *Danio rerio* is largely underestimated: evidence from the study of Ser/Arg-rich splicing factors

Marine Joris[1,*], Marie Schloesser[1], Denis Baurain[2], Marc Hanikenne[1], Marc Muller[3] and Patrick Motte[1,*]

[1]Laboratory of Functional Genomics and Plant Molecular Imaging, InBioS, PhytoSystems and Centre for Assistance in Technology of Microscopy (CAREm), University of Liège, 4000 Liège, Belgium, [2]InBioS–PhytoSYSTEMS, Eukaryotic Phylogenomics, University of Liège, 4000 Liège, Belgium and [3]Laboratory for Organogenesis and Regeneration, GIGA-Research, University of Liège, 4000 Liège, Belgium

Received February 16, 2017; Revised July 10, 2017; Editorial Decision July 11, 2017; Accepted July 13, 2017

ABSTRACT

Although the involvement of Ser/Arg-rich (SR) proteins in RNA metabolism is well documented, their role in vertebrate development remains elusive. We, therefore, elected to take advantage of the zebrafish model organism to study the SR genes' functions using the splicing morpholino (sMO) microinjection and the programmable site-specific nucleases. Consistent with previous research, we revealed discrepancies between the mutant and morphant phenotypes and we show that these inconsistencies may result from a large number of unsuspected inadvertent morpholino RNA targets. While microinjection of MOs directed against *srsf5a* (sMO*srsf5a*) led to developmental defects, the corresponding homozygous mutants did not display any phenotypic traits. Furthermore, microinjection of sMO*srsf5a* into *srsf5a*$^{-/-}$ led to the previously observed morphant phenotype. Similar findings were observed for other SR genes. sMO*srsf5a* alternative target genes were identified using deep mRNA sequencing. We uncovered that only 11 consecutive bases complementary to sMO*srsf5a* are sufficient for binding and subsequent blocking of splice sites. In addition, we observed that sMO*srsf5a* secondary targets can be reduced by increasing embryos growth temperature after microinjection. Our data contribute to the debate about MO specificity, efficacy and the number of unknown targeted sequences.

INTRODUCTION

SR proteins constitute a phylogenetically conserved family of RNA-binding proteins that are involved in many aspects of (pre-)mRNA metabolism. First described as constitutive and alternative splicing regulators, they are also implicated in transcription, non-sense-mediated decay, mRNA export, translational control as well as maintenance of genome stability (1–3). In order to clarify identification of SR splicing factors, a new definition has been proposed considering them as any protein with a modular structure consisting of one or two RNA recognition motif (RRM) at the N-terminus and a C-terminal Ser/Arg-rich domain (RS) of at least 50 amino acids with >40% RS or SR repeats (4). Based on their architecture, SR proteins can be divided into three subfamilies in vertebrates; (i) SRSF1-like (one RRM and one pseudo-RRM), (ii) SRSF2-like (one RRM) and (iii) SRSF7-like (one RRM and one 'zinc knuckle'). SR proteins have been shown to bind exonic splicing enhancers (ESEs) sequences on pre-mRNAs via their RRMs and to recruit spliceosomal components via their RS domain. SR proteins can function either as splicing activators (exon inclusion) or negative regulators (exon skipping), depending on the context (5,6). While some SR proteins seem to bind a small set of endogenous-specific targets, others share many binding sites suggesting a close collaboration between these proteins in mRNA metabolism (7,8). Whereas their functions at the molecular level are well documented, their roles in a physiological and developmental context are incompletely understood (9). The difficulties to uncover their function in a specific model may be tied to their essential role in cell viability (i.e. apoptosis and cell cycle progression) (10). Indeed, inactivation of several SR genes leads to death in early stages of embryo development in mouse and *drososophila*

*To whom correspondence should be addressed. Tel: +32 4 3663811; Fax: +32 4 3662960; Email: marine.joris@doct.ulg.ac.be
Correspondence may also be addressed to Patrick Motte. Tel: +32 4 3663810; Fax: +32 4 3662960; Email: patrick.motte@ulg.ac.be

(11,12). Furthermore, several SR genes have redundant developmental functions in *Caenorhabditis elegans* and their inactivation had little or no effects on *Caenorhabditis* development (13). To address this issue, we evaluated the *Danio rerio* model system. Antisense morpholino oligonucleotide microinjections permitted to obtain graded phenotypes (14) and genome editing was concomitantly used to generate stable knockout lines.

Morpholinos (MOs) consist in chemically modified short oligonucleotides (25 nt) that are able to bind RNA with natural complementary base pairing, while they contain a morpholine ring instead of ribose and non-ionic phosphodiamidate backbones (15). This particular MO architecture makes them nuclease-resistant with low toxicity (16). Whereas translation MOs inhibit ribosome binding to mRNAs, splicing MOs bind on pre-mRNA splice junctions and sterically block their recognition by spliceosomal components. The use of MOs was rapidly recognized as a powerful tool to investigate gene function during early embryonic development in a variety of organism including *Xenopus tropicalis*, *Mus musculus* and *Gallus gallus* (17–20). In zebrafish, MOs have been the most advocated technique to knockdown genes for the past decades (21). Recently, the emergence of new gene editing techniques like TALEN and CRISPR/Cas9 (22–25) reversed this trend and enabled researchers to rapidly and easily generate fish knockouts. The extensive generation of mutant lines has revealed discrepancies between mutant and morphant phenotypes, suggesting MOs off-target effects (26,27). It has been shown that these discrepancies can be explained by compensation mechanisms in knockout mutants (28).

Fifteen zebrafish SR genes were identified belonging to the three subfamilies of SR proteins (Supplementary Figure S1). In this study, we investigate the role of the splicing factor Srsf5a, displaying a specific expression profile and belonging to the extensively studied SRSF1 family. We observed that, while the microinjected MOs directed against *srsf5a* (sMO*srsf5a*) led to developmental defects, the corresponding homozygous mutants did not display any phenotypic traits. Furthermore, microinjection of sMO*srsf5a* into *srsf5a*$^{-/-}$ resulted in a phenotype as observed in the morphant. Similar findings were observed for two other SR genes (*srsf2b* and *srsf9*). Using deep mRNA sequencing, we found that these inconsistencies were likely due to several sMO*srsf5a* alternative target genes which could not be easily predicted by straightforward blast analysis. We also uncovered that only 11 consecutive bases complementary to the 25 MO bases are sufficient for binding and subsequent blocking of splice sites. In addition, we observed that sMO*srsf5a* secondary targets can be slightly reduced by increasing the growth temperature of embryos after microinjection. Our data contribute to the debate about MO specificity, efficacy and the number of unknown targeted sequences (14,29,30). Our findings also pave the way for more efficient identification of putative functional collateral MO target sites and moreover raise the question whether the experimental conditions used to perform MO, CRISPR/Cas9 or TALEN experiments could be optimized.

MATERIALS AND METHODS

Zebrafish breeding

Zebrafish (*D. rerio*) were raised and staged according to standard protocols (31). Embryos were kept in E3 medium with or without 0.003% 1-phenyl-2-thiourea at 28°C until harvested. They were fixed for 2 h in 4% paraformaldehyde and dehydrated in 100% methanol before analysis. All experiments and the entire study were evaluated by the Ethical Committee of the University of Liege, Belgium and accepted under the file number 1158.

Plasmids

Total RNA from 48 hpf embryos was extracted using TRIzol reagent (SigmaAldrich) and the RNeasy mini Kit (Qiagen), and reverse-transcribed using the RevertAid First Strand cDNA Synthesis Kit (ThermoFisher Scientific). The coding sequences: *srsf5a, srsf*5a/*Δ36, srsf5a-int3* and *mut-srsf5a-int3* were amplified from cDNAs (synthesized from uninjected, or sMO*srsf5a* injected wt and mutant embryos) by polymerase chain reaction (PCR) and cloned into pCS2plus Vector (Addgene) or in the pGEM®-T Easy Vector (Promega) for riboprobe synthesis. Primers used were listed in the Supplementary Table S6.

In vitro transcription

mRNA for injection were synthesized from pCS2plus after linearization by NotI using the mMESSAGEmMACHINE SP6 Kit (Ambion) and were purified by $LiCl_2$ precipitation. Riboprobes for *in situ* hybridization were synthesized from pGEM®-T Easy Vector using SP6 or T7 in a digoxigenin or DNP (2,4-dinitrophénol) labeling reaction. The zebrafish *isl-1* (ZDB-GENE-980526–112) and *pax6b* (ZDB-GENE-001031–1) probes were used.

In situ hybridization, H/E blade staining and image acquisition

In situ hybridization were performed as described (32). Anti-digoxigenin-HRP and anti-DNP-HRP were used with tyramide-Cy3 (Red) and tyramide-FITC (green) (Perkin-Elmer TSA Kit). Embryo cell nuclei were sometimes counterstained with 0.6 μM DRAQ7™. For H/E experiments, embryos were dehydrated in ethanol and embedded in a glycol methacrylate medium (Technovit® 7100). The 8-μm sections were obtained using a microtome (Leica) and were stained with hematoxylin and eosin according to standard protocols. Pictures were taken on a Nikon® Eclipse 90i microscope controlled by NIS-Elements microscope imaging software. Fluorescent images were acquired with a Leica® SP5 inverted confocal microscope.

Microinjections

Embryos were injected at the one cell stage into the yolk. Morpholinos were purchased from Gene Tools (Philomath, OR, USA). The sequences of the sMO*srsf5a*, sMO*srsf2b*; sMO*srsf9* and the CtrlMO are listed in Supplementary Table S6. MOs were injected at 3 ng for *srsf5a*, 2 ng for *srsf2b*

and for *srsf9*. The severity of the observed phenotype was MO dose dependent. The dose used in our experiments was the lowest one leading to the supposedly specific phenotype in 75% of embryos. For rescue or expression experiments, 50–200 pg of coding mRNA was injected. Morpholino and mRNA were each dissolved in 1× Danieau buffer containing 0.5% Tetramethylrhodamine dextran (Invitrogen, Belgium) to be able to sort well injected embryos under a fluorescent binocular. Based on developmental defect severity, MOs injected embryos were divided into three main classes; weak, intermediate and strong. The intermediate phenotype was the most frequently observed (in 75% of embryos, $n >$ 450) and was systematically used for further analysis. Each injection experiment was repeated at least three times using at least 150 individuals per experimental condition. No phenotypic differences were observed in sMO*srsf5a* morphants, in absence or presence of co-injection of a morpholino directed against p53 (33).

Western blot analysis

Proteins were extracted from 80 injected embryos (24 hpf). Samples were dissolved in Laemmli buffer before gel electrophoresis. A mouse monoclonal ANTI-FLAG® M2-Peroxidase (HRP) antibody (Sigma A8592) was used for detecting Flag-tagged protein using the BM chemiluminescence Western blot kit (Roche).

Genome editing

TALENs directed against *srsf5a* were designed using the TALE-NT software (https://tale-nt.cac.cornell.edu/) using the following criteria; spacer length: 15–20 bases, RVDs length: 15–20 bp. For each TALEN binding site, predicted targets were counted in the zebrafish genome. TALEN sequences were chosen for no off-target prediction (Supplementary Table S6). TALEN assembly in the right or left EF1α-SP6-TALEN expression vector was conducted using the FastTALE™ TALEN assembly kit from Sidansai Biotechnology. To produce TALEN mRNAs, left and right TALEN expression vectors were linearized by NotI and *in vitro* transcribed using the mMessageMachine SP6 kit (Ambion). About 50–200 pg of each TALEN mRNAs was injected as previously described. CRISPR directed against *srsf5b*, *srsf2b* and *srsf9* were designed and synthetized according to the Schier lab protocol (34,35) (Supplementary Table S6). DNA templates for sgRNAs *in vitro* synthesis using the Ambion MEGAscript T7 kit, were assembled by PCR using two oligos (Supplementary Table S7). Cas9 RNAs were generated using the pCS2plus-Cas9 plasmid (addgene) previously digest by NotI. Finally, 200–300 pg of Cas9 RNA and 50–100 pg of sgRNAs were injected at one cell stage.

Genotyping

Nuclease-microinjected embryos were raised and genotyped at minimum 2 months. DNA was extracted from fish fin clip. The sample was incubated in 150 μl of NaOH 50 mM solution for 10 min at 95°C, cooled down and neutralized with 1/10th volume of 1M Tris–HCl, pH 8. Genotyping was conducted using PCR followed by Heteroduplex Mobility shift Assay (HMA). Specific HMA PCR primers were designed to amplify a 120-bp region around the TALEN-targeted site (Supplementary Table S7). HMA was prepared by adding a 10× denaturing buffer (1M NaCl, 20 mM ethylenediaminetetraacetic acid, 100 mM Tris–HCl pH 7.8,) to the PCR product. The mixture was denatured at 100°C for 2 min and then cooled to 4°C for 10 min to permit the formation of heteroduplexes made of non-mutant and mutant PCR product. The samples were loaded on a 12% polyacrylamide gel and electrophoresis was carried out at 90 volts for 3 h in Tris Borate EDTA (TBE) buffer using a Biorad system and gel red stained. TALEN mutated fish were out-crossed to wild-type (wt) fish and the embryos were screened for germline mutations. F1 fish were genotyped at minimum 2 months and heterozygous fish were selected and sequenced to verify mutations. Mutants were then genotyped using primers to amplify a 70-nt region containing the deletion (Supplementary Table S7).

qPCR

Quantitative RT-PCR reactions were performed in 384-well plates with an ABI Prism 7900HT system (Applied Biosystems) using Maxima SYBR® Green qPCR Master Mix (Eurogentec) on material from three independent biological experiments (Figure 2B and Supplementary Figure S5), or from three independent mutant lines (Figure 2E) for each combination of cDNA and primer pair. Gene expression was normalized relative to *ef1alpha* and *rpl13alpha*. Supplementary Table S7 shows the primers used for these experiments.

RNA sequencing

Total RNA from 48 hpf control and sMO*srsf5a* embryos was extracted as described above. RNA sample quality and quantity were evaluated using both Bioanalyzer 2100 (Agilent) and Nanodrop. Libraries were prepared using the TruSeq kit (Illumina) and cDNA fragments ranging from 300 to 500 bp were selected and sequenced on a HiSeq2000 platform (Illumina) to generate 101-bp paired-end FASTQ sequences. Reads were mapped on the zebrafish genome (Zv9, Ensembl genome version 75, ensembl.org) using Tophat v.2.0.9 (-r 200, -p1, -m2, –solexa1.3-quals) (36). Gene expression was measured from the mapped reads by using HT-seq-count (intersection-strict mode) and differentially expressed (DE) genes were determined using the R package DESeq2 (37–39). MATS version 3.0.9 was used to detect differential alternative splicing events (-t paired -len 101 -a 8 -r1 178,176 –r2 183,195 -sd1 60,60 –sd2 61,67 –analysis P, a gtf file coming from the Zv9 version of the genome was also given to MATS) (40). Insert sizes were calculated using Picard Tools. Data are shown in Supplementary Tables S1 and 2. RNA-Seq data are submitted to GEO database under accession number GSE98888.

Blast analysis

Blast analysis were performed using NCBI/BLASTN on sequences coming from RNAseq data or Ensembl/BLASTN

against Zebrafish GRCz10 (Genomic sequence) using the following parameters: Word size for seeding alignments: 11, Match/Mismatch scores: 1,-2. The sMO*srsf5a* sequence was used as a query. Data are shown in Supplementary Tables S3–5.

RT-PCR

To visualize differential splicing due to sMO*srsf5a* microinjection, total RNAs were extracted from 48 hpf injected embryos at 28°C (at 33°C the embryos were stopped at 38.5 hpf, the equivalent of the 48 hpf stage) and were reverse transcribed using oligo(dT)$_{18}$. Specific primers were used to amplify a region of interest into blast predicted target genes (Supplementary Table S7).

Electrophoretic mobility shift assays

Synthetic 77 nt RNAs (see Supplementary Methods and Supplementary Table S6) were incubated at 90°C for 1 min and quickly chilled on ice for 2 min. A total of 4 pmoles of sMO*srsf5a* were incubated with various amount of RNAs (0.6, 1.2, 1.8, 2.4, 2.8 pmoles) in 10 μl of 1× TMN buffer (20 mM Tris-Acetate, pH7.6, 100 mM NaOAc, 5 mM Mg(OAc)$_2$) at 28°C for 15 min. Two microliters of 6× non-denaturing RNA loading buffer were added and the samples were run on a 11% non-denaturing polyacrylamide gel in 1× TBE at 90 V for 2 h. The gel was stained with GelRed™ (10 000×) for 10 min and visualized under UV.

RESULTS

Microinjection of MOs directed against *srsf5a* led to developmental defects

We first determined the expression profile of *srsf5a* by *in situ* hybridization (Supplementary Figure S2). Like many *D. rerio* SR genes (data not shown), *srsf5a* is maternally expressed and becomes widely expressed at later stages (24, 48 and 72 hpf) in the central nervous system and in the pharyngeal region. Noticeably, *srsf5a* displayed a more distinct expression in the developing eye, particularly in the ganglional cell layer and in the inner nuclear layer of the retina. These data led us to hypothesize that *srsf5a* could have a role in cell differentiation during eye formation.

To examine the role of Srsf5a during early embryonic development, we injected at one cell stage a splice site blocking morpholino (sMO*srsf5a*) targeting the exon3-intron3 junction of the *srsf5a* pre-mRNA (Figure 1A). At this dose, 95% ($n > 450$) of *srsf5a* morphant embryos suffered from developmental delay and poor swimming activity. We observed opaque areas in the brain and in the eyes, indicative of necrotic zones, reduction of pigmentation (visible at 48 hpf) and often bent tails and pericardial oedemas (in 30% of embryos) (Figure 1B). More thorough analysis revealed cell death in the brain and severe defects in the developing eye of morphants (Figure 1C and D). The apparent specificity of these defects for *srsf5a* knock-down was tested by co-injecting the sMO*srsf5a* with 80 pg of Srsf5a-coding mRNA which resulted in partial rescue of the embryonic morphant defects (Figure 1B and D). Remarkably, the *srsf5a* expression pattern largely coincided with the MO-induced phenotype.

Analysis of the *sMOsrsf5a* impact on *srsf5a* transcripts confirmed disruption of splicing at the targeted junction, causing retention of intron3 (*srsf5a-i3/153nt*) and consequently leading to the introduction of a premature STOP codon within the RRM1-encoding sequence. Moreover, it revealed a cryptic splice site located within exon3, inducing a deletion of 36 bases in the *srsf*5a open reading frame (*srsf*5a/*Δ36*) (Figure 1A). We therefore tested whether this splicing variant lead to synthesis of a mutant protein with a 12-amino acid deletion within the RRM1 domain by injecting a *srsf5a/Δ36*-Flag RNA. We did not observe any phenotypic consequences following *srsf5a/Δ36*-Flag mRNA injection, in contrast to injection of wt *srsf5a*-Flag mRNA (used as a control for overexpression) which caused drastic effects on embryonic development (Supplementary Figure S3) suggesting that *srsf5a/Δ36*-Flag RNA is inefficient at causing a defect and at leading to the synthesis of a mutant protein able to replace the wt protein function. At this stage of the study, our data strongly suggested that MO microinjection leads to partial inactivation of Srsf5a, leading to specific developmental defects.

In addition to the sMO*srsf5a*, four other MOs were used to knockdown *srsf5a* (trMO*srsf5a,* sMO*srsf5a2,* sMO*srsf5a3* and sMO*srsf5a4*; see Supplementary Method) but none of these could recapitulate the sMO*srsf5a* effects. No morphological defect was observed upon injection of trMO*srsf5a,* sMO*srsf5a2* and sMO*srsf5a3*, possibly because in all cases no difference in wt *srsf5a* mRNA levels could be detected. However, injection of sMO*srsf5a4* or co-injection of sMO*srsf5a3* and sMO*srsf5a4* led to brain necrosis, a high mortality rate and a decrease of wt *srsf5a* mRNA level (Supplementary Figure S4). Following these discrepancies between the effects of the different used MOs herein, we decided to generate stable knockout mutant lines by using TALEN (see below).

srsf5a$^{-/-}$ mutants failed to recapitulate the MOs induced phenotype

To concomitantly investigate the phenotype of stable *srsf5a* loss-of-function, we engineered two TALEN pairs and generated two *srsf5a* mutants in exon 2 (deletion of 11 nucleotides, Δ11) and exon 4 (deletion of 5 nucleotides, Δ5), respectively. In both cases, the mutation led to synthesis of a truncated protein theoretically missing domains critical for their function, due to premature STOP codons (Figure 2A). Analysis of the *srsf5a* transcript revealed an increased degradation rate in the two mutants compared to wt, confirming the efficacy of the mutation (Figure 2B, data not shown for *srsf5a*Δ5). Unexpectedly, these mutants failed to recapitulate the morphant phenotype (Figure 2C); no morphological defect could be observed at any embryonic stage and we obtained normal fertile homozygous adults (2-years-old). In the light of recently raised serious concerns about the use of MOs (26,27), a similar discrepancy was recently shown to result from genetic compensation in mutants through expression of a related protein (28). We therefore tested a putative complementation of the *srsf5a* mutation by other SR protein-encoding genes using quantitative RT-PCR (qRT-PCR). Expression levels of the 13 zebrafish SR genes were compared between offspring ob-

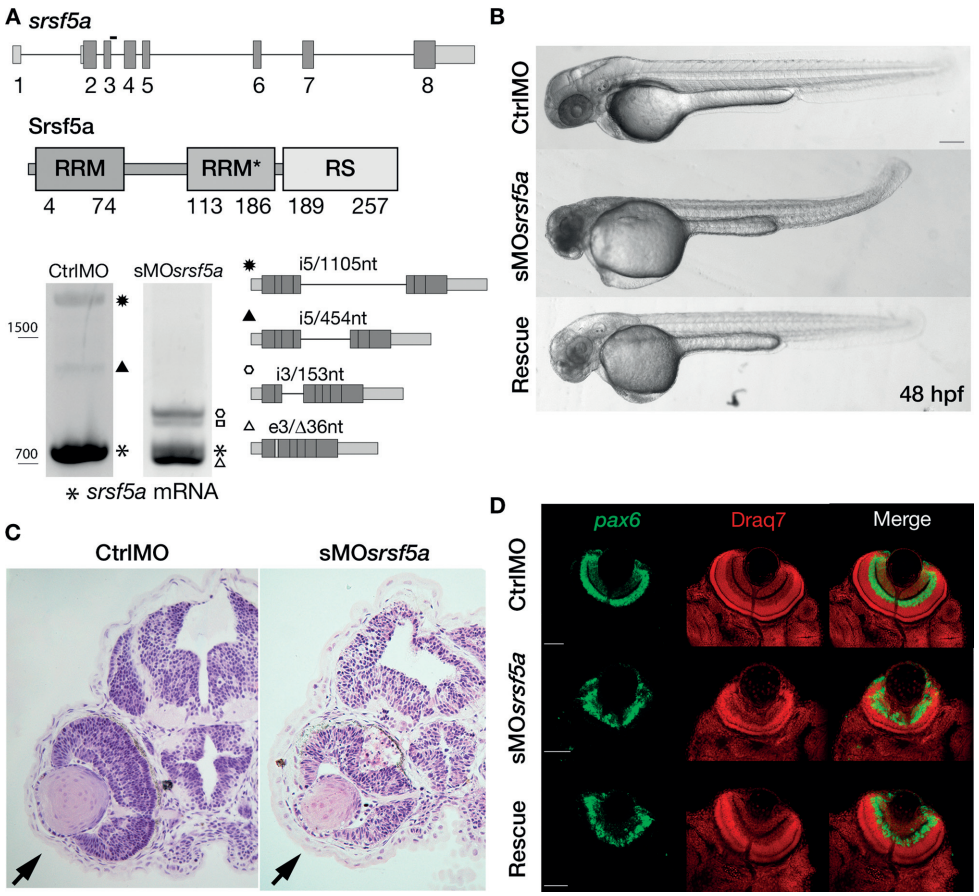

Figure 1. Injection of a splice site blocking MO targeting the *srsf5a* gene led to developmental defects. (**A**) *srsf5a* is composed of eight exons. The protein is encoded by exons 2–8 and consists of two RRM domains responsible for RNA binding and one RS domain, essential for protein–protein interactions. Three different transcripts are produced from *srsf5a*. Among them, two alternative transcripts retain intron 5 or a part of it (black up-pointing triangle and black dot). sMO*srsf5a* was designed to target the exon3–intron3 junction. RT-PCR experiments to amplify *srsf5a* mRNA in control and morphant embryos at 48 hpf revealed intron3 retention (open hexagon mark), introducing a premature STOP codon into the RRM1 encoding part of the mRNA. Expression of the three normal *srsf5a* transcripts was strongly reduced in morphants, while MO injection also triggered the use by the splicing machinery of a cryptic splice site located in exon3, and leading to a deletion of 36 bases in the open reading frame of the *srsf5a* transcript (*srsf*5a/*Δ36,* open triangle mark). The resulting protein has a 12-amino acids deletion within the RRM1. The open square mark corresponds to a *srsf5a* transcript in which intron3 is retained and with a deletion of 36 bases in the exon3 (*srsf*5a/*Δ36-intron3).* All PCR products were identified by sequencing. (**B**) Zebrafish embryos injected with 3 ng of ctrlMO or sMO*srsf5a* with or without a rescuing dose of *srsf5a* mRNA (80 pg) at 48 hpf. The defects in brain, eye and curved tail could be partially rescued by *srsf5a* mRNA injection. Pigmentation was not visible as embryos were treated with 1-phenyl-2-thiourea to increase their transparency. Bar: 200 μm. (**C**) Haematoxylin/eosin sections obtained from ctrlMO and sMO*srsf5a* injected embryos revealed abnormal organization of cells in the retina and an increase of cell death in the eye and the entire brain at 48 and 72 hpf (data not shown). (**D**) Fluorescent *in situ* hybridization using a *pax6b* probe followed by nuclear staining using draq7® revealed the disorganization of the ganglional cell layer and of the inner nuclear layer in the retina at 72 hpf in morphants compared to control embryos. Rescue experiments allowed us to partially restore the control phenotype. Scale bar: 50 μm.

tained from homozygous mutants or from wt parents. We observed an increased expression of *srsf1b*, *srsf2b, srsf3a, srsf5b* and *srsf6a* in 24 hpf mutant larvae and of *srsf3a* at 48 and 72 hpf (Figure 2B and Supplementary Figure S5). In *srsf5a* homozygous mutant embryos born from an incross of heterozygous parents, no change in SR gene expression could be detected, likely due to maternally provided *srsf5a* mRNA (Supplementary Figure S5). In contrast, none of these SR gene overexpressions was observed in morphant embryos (Figure 2B). Taken together, these results suggest that compensatory mechanisms may be responsible for the lack of phenotype in *srsf5a* mutants. Interestingly, double *srsf5a*/*srsf5b* homozygous mutants were generated and did not display any developmental defect, suggesting that inactivation of only the closest relative would not be sufficient to overcome such a compensation effect. Comparison of SR gene expression levels in *srsf5b*$^{-/-}$ and wt at 24 hpf also revealed an overexpression of *srsf3a*, proposing a central role for this factor in compensation mechanism (Figure 2D and E).

Evidence of MO non-specificity

Further investigations were therefore required to understand the reasons for the contradictory results observed between morphants and mutants. We injected sMO*srsf5a* in *srsf5a* mutant embryos and strikingly, these embryos displayed the same defects as observed in wt morphants (Supplementary Figure S6a), arguing against a mechanism where MO injection simply blocks Srsf5a expression in

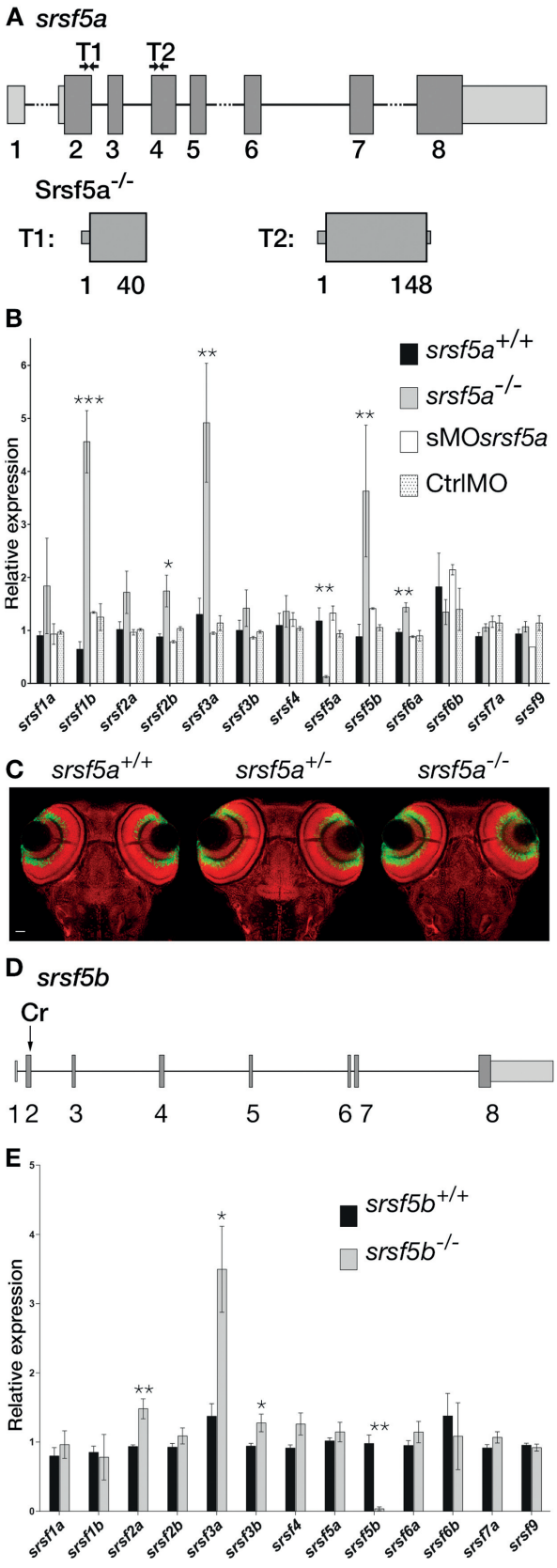

Figure 2. *srsf5a*$^{-/-}$ *and srsf5b*$^{-/-}$ did not show any developmental defects, but presented an overexpression of several homologous *SR* genes. (**A**) Two TALEN pairs were designed to target exon 2 or exon 4 of the *srsf5a* locus. TALEN pairs 1 and 2 generated of a deletion of, respectively 11 (Δ11) and 5 nt (Δ5), resulting in the production of a protein truncated in the RRM1 domain. (**B**) Quantitative RT-PCR to measure mRNA expression of *sr* genes in wild-type (wt), *srsf5a* mutants, morphants and ctrlMO microinjected embryos at 24 hpf. A strong decrease of *srsf5a* mRNA levels was observed in mutants compared to wt, suggesting the loss of Srsf5a protein in the mutant. In contrast, an upregulation of *srsf1b*, *srsf2b*, *srsf3a, srsf5b* and *srsf6a* was found. No such differences were observed in morphants compared to injected control embryos or wt. The data represent mean ± S.D. expression relative to the *ef1alpha* reference gene of at least three independent experiments. One-way ANOVA followed by a Tukey's multiple comparison test was used for statistical analysis. *, **, ***Mutants are statistically different from wt (*$P \leq 0.05$, **$P \leq 0.01$ and ***$P \leq 0.001$). (**C**) Fluorescent *in situ* hybridization using a *pax6b* probe followed by nuclear staining using draq7® in *srsf5a*$^{-/-}$ mutants and wt. No phenotype could be detected. (**D**) A CRISPr (Cr) was designed to target *srsf5b* exon2 and allowed us to obtain three different *srsf5b* mutants presenting 5, 11 or 14 bases deletion. The three mutations led to the production of a truncated protein in the RRM1 domain. (**E**) Comparison of SR genes expression level between *srsf5b* homozygous mutants (including the three mutant lines) and wt embryos at 24 hpf showed an overexpression of *srsf2a*, *srsf3a* and *srsf3b.* A drastic decrease of *srsf5b* expression confirmed its depletion in mutants. All data are expressed as the mean ± SEM. A one-way ANOVA was used for statistical analysis, followed by a multiple comparison Tukey's test. *, **, *** Mutants are statistically different from wt (*$P \leq 0.05$, **$P \leq 0.01$).

wt. Similar results were obtained in otherwise unaffected *srsf2b* (one RRM) and *srsf9* (one RRM and one pseudo-RRM) mutants; microinjection of the corresponding MOs produced the same effects in wt or mutant embryos (Supplementary Figure S7). Analysis of the *srsf5a* mRNA in sMO*srsf5a*-injected mutant larvae revealed the presence of the previously observed *srsf*5a/*Δ36* mRNA, and an unexpected accumulation of the *srsf5a-i3/153nt* variant (Supplementary Figure S6b). To test for the possibility that this latter mRNA could be responsible for the morphant phenotype, e.g. by acting as a non-coding RNA (41) or as a mutant protein by using an alternative start codon (42), we injected the *srsf5a-i3/153nt*-Flag mRNA into mutant eggs. No effect was observed during embryonic development (Supplementary Figure S6c) and no protein production could be observed (Supplementary Figure S6d).

MOs: a plethora of secondary targets

Taken together, our data strongly suggest that the effects caused by the sMO*srsf5a* result from its action on one or several alternative targets. Therefore, we performed RNA sequencing analysis on mRNA extracted from control and morphant embryos. We identified 1006 DE genes and 378 differentially spliced (DS) transcripts (Supplementary Tables S1 and 2). First, we blasted the sMO*srsf5a* sequence against the genomic sequences of DE or DS genes extracted using BiomaRt (43) and we obtained two lists resuming the most homologous sequences (*E*-value < 73) (Supplementary Tables S3 and 4). Next, we analyzed the position of these sequences within genes and we could point out many sequences localized on splice junctions, the best place for MOs to perturb splicing and consequently gene expression (Figure 3). In the DE gene list, 8 matching sequences are localized on exon-intron junctions whereas in blast results us-

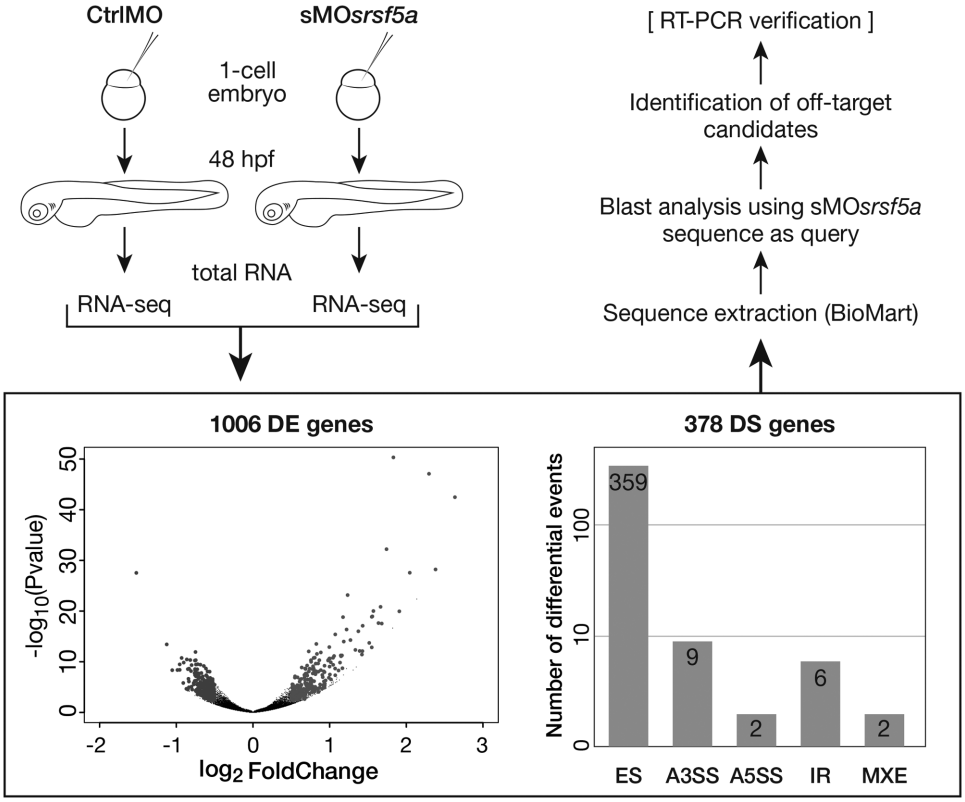

Figure 3. Process to determine secondary target RNAs for sMO*srsf5a*. CtrlMO and sMO*srsf5a* were injected at one cell stage. Total RNAs were extracted at 48 hpf and were processed according to the standard Illumina protocol, including TrueSeq mRNA library construction and sequencing in HiSeq 2000 (2 × 101 nt paired-end sequencing). A volcano plot summarizes RNAseq analysis in which 1006 genes were identified as statistically differentially expressed (DE) between control and morphant embryos. Right gray dots represent overexpressed genes (log_2FoldChange > 0.5, padjust < 0.05), while left gray dots represent underexpressed genes in morphants (log_2FoldChange < −0.5, padjust < 0.05). The bar plot recapitulates the number of differentially alternative splicing events (DS transcripts) detected by MATS when comparing control and MO*srsf5a* transcriptomes. Sequences from these DE genes and DS transcripts were extracted using BioMart and used as subjects in a blast analysis with the sMO*srsf5a* sequence as a query. The resulting lists (Supplementary Table S4) were scanned manually to find target regions localized on a splice junction. ES, Exon Skipping; A3SS, 3′ Splice Site; A5SS, 5′ Splice Site; IR, Intron Retention; MXE, Mutually exclusive exons.

ing DS genes, 19 sequences spanning spliced junctions were identified.

To determine whether the sMO*srsf5a* could indeed affect splicing by binding to the identified sequences, RT-PCR was performed on eight associated putative inadvertent mRNAs. For 6 of them, RT-PCR analysis confirmed the splicing defect in sMO*srsf5a* mRNA, even though only 11–15 successive bases out of the sMO*srsf5a* 25 bases are complementary to the tested pre-mRNAs (Figure 4 and Supplementary Figure S8). RNA sequencing allowed us to identify new spliced transcripts in morphants and the majority of them consisted in 'exon skipping events'. In many cases, these events imply exons located beside the junction containing a potential sMOsrsf5a binding sequence suggesting that these events are due to morpholino inadvertent binding (Supplementary Table S4). Interestingly, we also found three homologous sequences localized inside skipped exon in morphants (RNA-seq data) indicating that sMO*srsf5a* can influence the splicing independently of its splice junction binding (Supplementary Table S4). To make sure that these altered splicing events are not due to the partial decrease of Srsf5a expression, we analyzed mRNAs from the sMO*srsf5a3* or coinjected sMO*srsf5a3*/ sMO*srsf5a4* that were previously shown to decrease the levels of wt *srsf5a* mRNAs (Supplementary Figure S4A). In three randomly selected RNAs from the above list, no altered splicing was detected (Supplementary Figure S4B).

When sMO*srsf5a*-injected eggs were incubated at 33°C instead of the recommended 28°C (31), this slight increase in temperature resulted in some cases in a nearly complete absence of splicing defects (Figure 4 and Supplementary Figure S8) and less pronounced developmental defects in morphants (not shown).

The binding of sMO*srsf5a* to these inadvertent targets was also confirmed *in vitro* using electrophoretic mobility shift assay (EMSA). In this test, we mix the sMO*srsf5a* with its putative target RNA sequences and analyze the resulting duplex formation on a polyacrylamide gel (Figure 5 and Supplementary Figure S9). We could observe duplex formation of sMO*srsf5a* with the unspliced *srsf5a* sequence, but not with a sequence mutated at every second position in the sequence. Duplexes were also observed with the wt unspliced sequences of three randomly selected inadvertent targets, and with the wt spliced *srsf5a* sequence.

Taken together, these observations indicate that the defects observed in sMO*srsf5a* morphants are mainly due

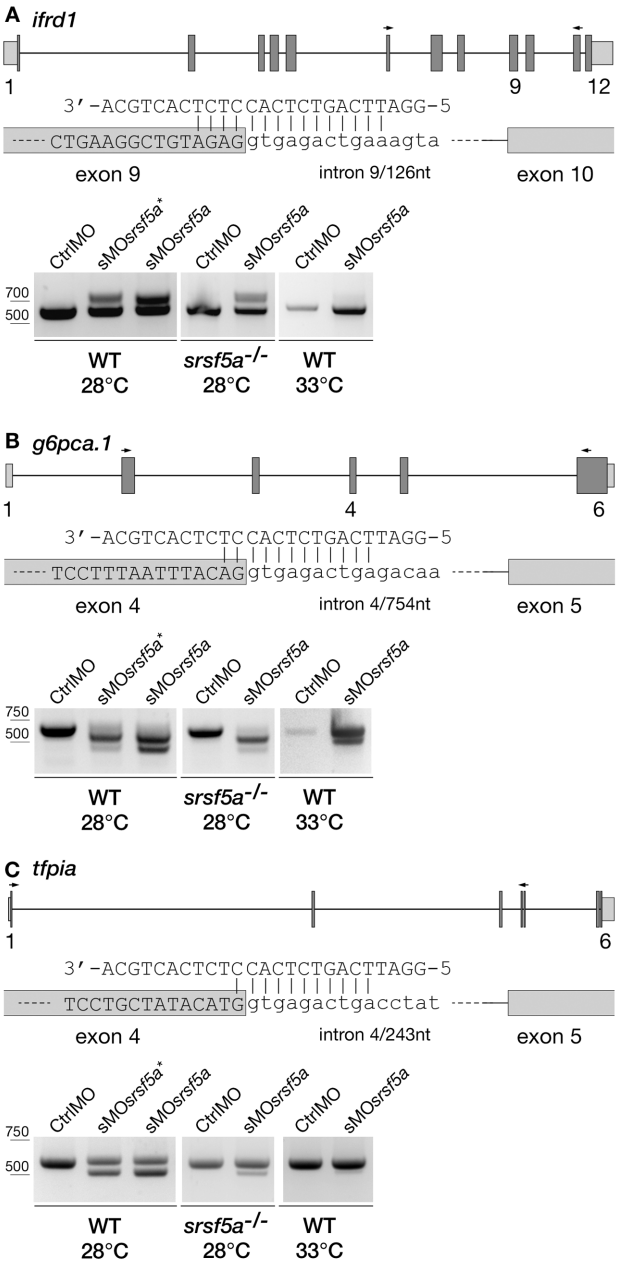

Figure 4. Injection of sMO*srsf5a* disturbed splicing of secondary target genes. (**A**) Schematic of the *ifrd1* splicing junction presenting 15 contiguous bases complementary to the morpholino. RT-PCR analysis using primers targeting exons 6 and 11 of *ifrd1* confirmed intron 9 retention due to sMO*srsf5a* binding. When the injected embryos were incubated at 33°C, retention of intron 9 was abolished. In *srsf5a*$^{-/-}$, splicing is disturbed as observed for wt embryos in response to sMO*srsf5a* injection. (**B**) Splicing of the *g6pca.1* gene was also affected by morpholino binding on 12 contiguous bases. Primers used to perform RT-PCR targeted the exon 2 and 6. (**C**) Amplification of *tfpia* mRNA (from exon1 to exon5) in control and morphant embryos revealed the existence of an exon skipping event in sMOsrsf5a injected embryos showing 11 bases are sufficient for MO binding. sMO*srsf5a**, embryos were injected with 2 ng of sMO*srsf5a*; sMO*srsf5a*, embryos were injected with 3 ng of sMO*srsf5a*.

to the binding of the 25bp MO to RNA sequences of a plethora of unrelated pre-mRNAs at 28°C rather than to the inactivation of *srsf5a.*

DISCUSSION

SR genes regulatory network

Herein, we attempt to study SR protein functions during zebrafish embryonic development. For this purpose, we used MO microinjection and TALENs/CRISPR gene editing techniques to generate stable knockouts. Our data revealed that injection of MOs against *srsf5a*, *srsf2b* or *srsf9* led to developmental defects that could not be recapitulated in the corresponding mutants. These observations are somehow consistent with recent data showing poor correlation between morphant and mutant phenotypes (26). Similar data have been previously reported in mouse, *Drosophila* and *Arabidopsis thaliana* when comparing knockout and knockdown results (44–46). Recently, Rossi *et al.* demonstrated the implementation of a compensatory network in response to deleterious mutations performed in the zebrafish genome (28). This compensatory network was not activated upon gene knockdown, explaining why MOs led to many overt phenotypes while mutants did not.

We reasonably asked whether at least one of the fifteen *D. rerio* SR proteins could take over the Srsf5a developmental function. Quantification of SR gene expression levels in *srsf5a*$^{-/-}$ compared to control and morphant embryos revealed an induced expression of *srsf1b*, *srsf2b, srsf3a, srsf5b* and *srsf6a*. We could similarly observe an overexpression of *srsf3a* in *srsf5b*$^{-/-}$. These findings prove the existence of a regulatory signaling cascade triggered by SRSF loss-of-function and converging on expression of other SR protein genes during embryonic development. Although we could not provide the insight into SR protein functions during early vertebrate development, our results reveal the compensatory mechanisms in mutants which have not been previously described for SR proteins. Interestingly, a recent RNA-mapping study revealed that mouse SRSF1 and SRSF2 exhibit extensive overlap in their RNA targets and that loss of RNA binding by one SR protein induces compensatory changes in RNA binding by another SR protein (7). Similarly, recent works in *Drosophila* showed that SR proteins act in a combinatorial manner to regulate splicing (i.e. exon inclusion and skipping) (6). Despite its different structural composition (one RRM versus two RRMs), Srsf3a seems to be a central regulator in compensation mechanism. Further studies will be required to identify the RNA targets of individual SR protein and to understand how different SR proteins can play cooperative (or redundant) roles in splicing in living organisms. Our findings call for a thorough investigation of the SR protein-specific interaction network regulating mRNA splicing during vertebrate development.

MO RNA inadvertent target

Despite possible compensatory mechanisms, we could recapitulate the morphant phenotype in stable mutant embryos (therefore lacking MO binding sites) suggesting other explanations for phenotypic discrepancies. The same observa-

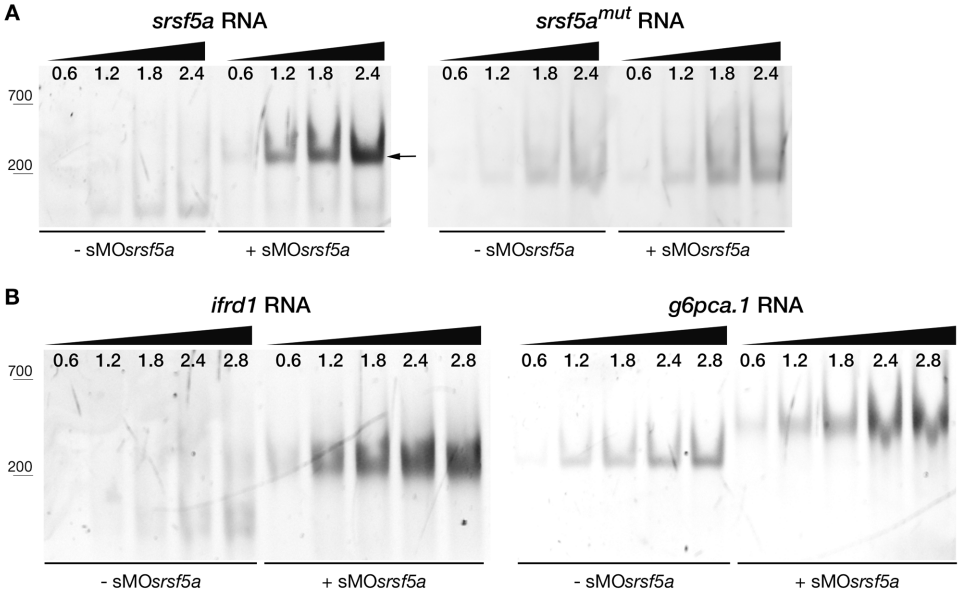

Figure 5. Detection of sMO*srsf5a*–RNAs interactions by EMSA. Various amount of RNAs (from 0.6 to 2.8 pmoles) were incubated with (+sMO*srsf5a*) or without (−sMO*srsf5a*) 4 pmoles of morpholino. (**A**) Two 77-nt RNAs containing either the morpholino binding site of *srsf5a* (*srsf5a* RNA) or a mutated binding site (*srsf5a*^{mut} RNA) were run on an 11% native polyacrylamide gel. In case of sMO*srsf5a* binding to the RNA, a shift was observed due to duplex formation (see arrow). The *srsf5a* RNA was bound by the morpholino (positive control) while the mutated *srsf5a* RNA was not (negative control). (**B**) sMO*srsf5a* was able to bind *ifrd1* RNA via its 15 bases complementary sequence. Interaction between sMO*srsf5a* and the 12 contiguous bases of the *g6pca.1* RNA was also assayed.

tions have been reported for the *megamind* mutant (26,47). Many causes for such inconsistencies have been proposed including hypomorphic alleles, maternal contribution or off-target effects. In our study, the first two hypotheses were unlikely: (i) qPCR data confirmed an increased degradation rate of *srsf5a*$^{-/-}$ transcripts suggesting the absence of Srsf5a proteins, and (ii) we used splicing MOs that only act on zygotic transcripts. MO-induced defects were likely due to off-target effects.

A major concern about the use of sequence-specific knockout and knockdown techniques is unwanted sequence binding. With the expansion of genomic and transcriptomic data, many algorithms were designed to predict associated MO or sgRNA inadvertent targets. A method called Genome-wide Unbiased Identification of Double Strand Breaks Enabled by Sequencing showed recently that blast-based methods were unable to efficiently predict real off-targets for CRISPR RNA-guided nucleases (48). Indeed, the majority of identified binding sites for sMO*srsf5a* using mRNA sequencing were not (easily) detected by a simple straightforward blast analysis.

MOs are supposed to be virtually free of off-target effects achieving an exquisite sequence specificity (15). They are neutral and unable to electrostatically interact with proteins. Moreover, their calculated minimum inhibitory lengths (MIL) are supposed to contain sufficient sequence information to ensure targeting of a unique transcript. Using deep mRNA sequencing, we identified DE genes and DS transcripts in sMO*srsf5a* injected embryos. Their corresponding sequences were used for downstream blast analysis to identify several potential *srsf5a* MO-binding sites spanning a splice junction. RT-PCR analysis detected new splice variants for DE genes, thus confirming inadvertent binding of sMO*srsf5a*. New alternative splicing events due to MO inadvertent binding were also validated by MATS analysis of transcriptomic data. Although previous work already theorized that MOs have a MIL value of 14–15 contiguous bases (at 37°C) (15), we show here that, at 28°C, the MIL is decreased down to 11 nt. Experiments in sea urchin embryo culture are performed at 14°C, suggesting an even much lower MIL value which may explain the already reported off target effects in sea urchin embryos injected with MOs (49). Despite the so-called 'exquisite' sequence specificity of MOs, we have established its effect on secondary target mRNAs in the zebrafish genome. The number of these unintended RNA targets may be largely underestimated, especially because MOs act at a rather low temperature in the zebrafish model. The influence of MOs on non-coding RNA (i.e. miRNAs, lncRNAs) or on regulatory exonic and intronic sequences (in which similar homology stretches of 11 nt might exist) has never been evaluated. Our study suggests a new mechanism of MOs action by which they influence splicing regardless of their binding to splice junctions. Indeed, by binding within an exon, they may affect the splicing process by hiding ESEs or ESSs (exonic splicing silencers) and inhibiting *trans* splicing factor binding. At last, the relatively high number of conserved positions at the 5′-splice sites increases the likelihood of finding imperfect MO-binding sites at splicing junctions in other RNAs. Similarly, translation MOs are systematically designed to target the conserved Kozak and AUG sequences. By computational analysis and based on the observed MIL value of 11, we determined the probable number of sMO*srsf5a*'s secondary

targets located on introns, exons and exon-intron junctions in the zebrafish genome. To this end, we searched perfect matches between the reverse complemented MO sequence (5′-TGCAGTGAGAGGTGAGACTGAATCC-3′) and all pre-mRNA sequences (see Supplementary Methods). We were able to find 279, 1822 and 489 matches in exons, introns and junctions respectively (Supplementary Table S5). For statistical assessment of sMO*srsf5a* preference for junctions over exons and introns, the same search was performed on 200 sets of random background sequences controlled for either the mononucleotide or dinucleotide composition. When using these simulated pre-mRNA sequences, the number of matches found on introns and exons did not significantly decrease (1.35- to 2.56-fold), in contrast to the number of matches found on junctions (44.66- to 59.09-fold) (Supplementary Table S5). These results clearly indicate that the presence of conserved junction sequences should be taken into account in MO sequence design. From these data, we propose two ways for reducing MO binding to secondary targets: (i) by promoting the use of a relatively high incubation temperature in order to increase stringency and indeed the k-value (Supplementary Table S5) and (ii) by preventing the presence of residues complementary to the highly conserved splice sequences (AG-GUNAG at the donor site and C/UAG-G/A at the acceptor site) by targeting (if at all possible) known regulatory intronic/exonic sequences (50) in the MO.

Does rescue mean 'no off-target'?

RNA rescue experiments have been thought to be a robust control to approve MO specificity. However, morphant embryos have been rescued in many studies reporting phenotype inconsistencies (27,30). In most of these studies using a splice site morpholino, the phenotype was rescued using a mature spliced mRNA missing a considerable part of the MO target sequence. Our work suggests that sMO*srsf5a* binding to 13 consecutive bases of the co-injected mRNAs can provide an explanation for any rescue by decreasing knockdown efficiency due to sMO*srsf5a* titration (26). This hypothesis was confirmed in vitro using EMSA (Supplementary Figure S9). Sequential rescue experiments were performed, intending to decrease this titration phenomenon, by injecting the mRNA at the one-cell stage and the MO at the 4-cells stage. However, partial rescue still occurred, suggesting that the injection delay is not sufficient *per se* for preventing MO binding to the injected RNA (Supplementary Figure S10). Given the high copy number of injected MOs and RNAs, we hypothesize that they can still hybridize in the embryo cells. The more severe phenotype observed in *srsf5a*$^{-/-}$ injected embryos could be explained by a more important sMO*srsf5a* binding to inadvertent RNAs due to the absence of *srsf5a* mRNAs.

Many other standard controls were recommended to check MO specificity (51). Several different MOs should be tested, although functional analysis of SpRunt in sea urchin provided a cautionary example of the insufficiency of two different morpholinos as a control for specificity (49). The use of a five-base mismatch control MO was also suggested. With only 11 nt being sufficient for effective binding, such controls appear somehow problematic. Mismatches should be designed along the entire MO sequence to interrupt any 11 nt inadvertent complementarity stretch; however this does not avoid appearance of new unintended target sites. Therefore, we also think that the only valid control of MO specificity might be the confirmation that its effects are lost in a null background (29). On the other hand, studies using mutants may suffer from masking of the correct phenotype by compensatory mechanisms, as also illustrated here. In such a case, MOs may be useful as they seem unable to trigger the compensatory response, if their specificity is sufficiently proven, and if the 11-nt MIL value is considered. With all these precautions, mutants combined with antisense MOs represent a valid toolbox to elucidate the true function of a gene.

SUPPLEMENTARY DATA

Supplementary Data are available at NAR Online.

ACKNOWLEDGEMENTS

We thank Steven Fanara for helpful discussions. We also want to thank the zebrafish facility of the GIGA-R center. *Author contributions:* P.M. and M.M. conceived the project and secured funding. M.J., P.M. and M.M. coordinated the study and designed experiments. M.J. and M.S. performed the experiments. D.B. performed the statistical analysis about the number of sMO*srsf5a* RNA secondary targets within the zebrafish transcriptome. The paper was written and figures prepared by M.J., P.M. and M.M. All authors interpreted and discussed the results, and commented on the manuscript.

FUNDING

'Fonds National de la Recherche Scientifique—FNRS' [FRFC n°2.4631.11F, CDR J.0080.15 to D.B.]; 'Fonds Spéciaux du Conseil de la Recherche' from the University of Liège; FRIA (Fonds de la Recherche pour l'Industrie et l'Agriculture, Belgium Doctoralship (to M.J.)); University of Liège 'Crédit de démarrage 2012′ SFRD-12/04 (to D.B.); Chercheur Qualifié du F.N.R.S. (Fonds National de la Recherche Scientifique, Belgium) (to M.H., M.M.). Funding for open access charge: Fonds De La Recherche Scientifique—FNRS and University of Liège .
Conflict of interest statement. None declared.

REFERENCES

1. Zhong,X.Y., Wang,P., Han,J., Rosenfeld,M.G. and Fu,X.D. (2009) SR proteins in vertical integration of gene expression from transcription to RNA processing to translation. *Mol. Cell*, **35**, 1–10.
2. Long,J.C. and Caceres,J.F. (2009) The SR protein family of splicing factors: master regulators of gene expression. *Biochem. J.*, **417**, 15–27.
3. Howard,J.M. and Sanford,J.R. (2015) The RNAissance family: SR proteins as multifaceted regulators of gene expression. *Wiley Interdiscip. Rev. RNA*, **6**, 93–110.
4. Manley,J.L. and Krainer,A.R. (2010) A rational nomenclature for serine/arginine-rich protein splicing factors (SR proteins). *Genes Dev.*, **24**, 1073–1074.
5. Fu,X.D. and Ares,M. Jr (2014) Context-dependent control of alternative splicing by RNA-binding proteins. *Nat. Rev. Genet.*, **15**, 689–701.

6. Lee,Y. and Rio,D.C. (2015) Mechanisms and Regulation of Alternative Pre-mRNA Splicing. *Annu. Rev. Biochem.*, **84**, 291–323.
7. Pandit,S., Zhou,Y., Shiue,L., Coutinho-Mansfield,G., Li,H., Qiu,J., Huang,J., Yeo,G.W., Ares,M. Jr and Fu,X.D. (2013) Genome-wide analysis reveals SR protein cooperation and competition in regulated splicing. *Mol. Cell*, **50**, 223–235.
8. Bradley,T., Cook,M.E. and Blanchette,M. (2015) SR proteins control a complex network of RNA-processing events. *RNA*, **21**, 75–92.
9. Anko,M.L. (2014) Regulation of gene expression programmes by serine-arginine rich splicing factors. *Semin. Cell Dev. Biol.*, **32**, 11–21.
10. Li,X., Wang,J. and Manley,J.L. (2005) Loss of splicing factor ASF/SF2 induces G2 cell cycle arrest and apoptosis, but inhibits internucleosomal DNA fragmentation. *Genes Dev.*, **19**, 2705–2714.
11. Ring,H.Z. and Lis,J.T. (1994) The SR protein B52/SRp55 is essential for Drosophila development. *Mol. Cell. Biol.*, **14**, 7499–7506.
12. Jumaa,H., Wei,G. and Nielsen,P.J. (1999) Blastocyst formation is blocked in mouse embryos lacking the splicing factor SRp20. *Curr. Biol.*, **9**, 899–902.
13. Longman,D., Johnstone,I.L. and Caceres,J.F. (2000) Functional characterization of SR and SR-related genes in Caenorhabditis elegans. *EMBO J.*, **19**, 1625–1637.
14. Blum,M., De Robertis,E.M., Wallingford,J.B. and Niehrs,C. (2015) Morpholinos: antisense and sensibility. *Dev. Cell*, **35**, 145–149.
15. Summerton,J.E. (2007) Morpholino, siRNA, and S-DNA compared: impact of structure and mechanism of action on off-target effects and sequence specificity. *Curr. Top. Med. Chem.*, **7**, 651–660.
16. Corey,D.R. and Abrams,J.M. (2001) Morpholino antisense oligonucleotides: tools for investigating vertebrate development. *Genome Biol.*, **2**, 1015.1–1015.3.
17. Nutt,S.L., Bronchain,O.J., Hartley,K.O. and Amaya,E. (2001) Comparison of morpholino based translational inhibition during the development of Xenopus laevis and Xenopus tropicalis. *Genesis*, **30**, 110–113.
18. Kos,R., Reedy,M.V., Johnson,R.L. and Erickson,C.A. (2001) The winged-helix transcription factor FoxD3 is important for establishing the neural crest lineage and repressing melanogenesis in avian embryos. *Development*, **128**, 1467–1479.
19. Coonrod,S.A., Bolling,L.C., Wright,P.W., Visconti,P.E. and Herr,J.C. (2001) A morpholino phenocopy of the mouse mos mutation. *Genesis*, **30**, 198–200.
20. Ekker,S.C. (2000) Morphants: a new systematic vertebrate functional genomics approach. *Yeast*, **17**, 302–306.
21. Nasevicius,A. and Ekker,S.C. (2000) Effective targeted gene 'knockdown' in zebrafish. *Nat. Genet.*, **26**, 216–220.
22. Kim,H. and Kim,J.S. (2014) A guide to genome engineering with programmable nucleases. *Nat. Rev. Genet.*, **15**, 321–334.
23. Irion,U., Krauss,J. and Nusslein-Volhard,C. (2014) Precise and efficient genome editing in zebrafish using the CRISPR/Cas9 system. *Development*, **141**, 4827–4830.
24. Hoshijima,K., Jurynec,M.J. and Grunwald,D.J. (2016) Precise editing of the zebrafish genome made simple and efficient. *Dev. Cell*, **36**, 654–667.
25. Gaj,T., Gersbach,C.A. and Barbas,C.F. 3rd (2013) ZFN, TALEN, and CRISPR/Cas-based methods for genome engineering. *Trends Biotechnol.*, **31**, 397–405.
26. Kok,F.O., Shin,M., Ni,C.W., Gupta,A., Grosse,A.S., van Impel,A., Kirchmaier,B.C., Peterson-Maduro,J., Kourkoulis,G., Male,I. *et al.* (2015) Reverse genetic screening reveals poor correlation between morpholino-induced and mutant phenotypes in zebrafish. *Dev. Cell*, **32**, 97–108.
27. Law,S.H. and Sargent,T.D. (2014) The serine-threonine protein kinase PAK4 is dispensable in zebrafish: identification of a morpholino-generated pseudophenotype. *PLoS One*, **9**, e100268.
28. Rossi,A., Kontarakis,Z., Gerri,C., Nolte,H., Holper,S., Kruger,M. and Stainier,D.Y. (2015) Genetic compensation induced by deleterious mutations but not gene knockdowns. *Nature*, **524**, 230–233.
29. Stainier,D.Y., Kontarakis,Z. and Rossi,A. (2015) Making sense of anti-sense data. *Dev. Cell*, **32**, 7–8.
30. Lawson,N.D. (2016) Reverse Genetics in Zebrafish: Mutants, Morphants, and Moving Forward. *Trends Cell Biol.*, **26**, 77–79.
31. Kimmel,C.B., Ballard,W.W., Kimmel,S.R., Ullmann,B. and Schilling,T.F. (1995) Stages of embryonic development of the zebrafish. *Dev. Dyn.*, **203**, 253–310.
32. Thisse,C. and Thisse,B. (2008) High-resolution in situ hybridization to whole-mount zebrafish embryos. *Nat. Protoc.*, **3**, 59–69.
33. Robu,M.E., Larson,J.D., Nasevicius,A., Beiraghi,S., Brenner,C., Farber,S.A. and Ekker,S.C. (2007) p53 activation by knockdown technologies. *PLoS Genet.*, **3**, e78.
34. Gagnon,J.A., Valen,E., Thyme,S.B., Huang,P., Akhmetova,L., Pauli,A., Montague,T.G., Zimmerman,S., Richter,C. and Schier,A.F. (2014) Efficient mutagenesis by Cas9 protein-mediated oligonucleotide insertion and large-scale assessment of single-guide RNAs. *PLoS One*, **9**, e98186.
35. Montague,T.G., Cruz,J.M., Gagnon,J.A., Church,G.M. and Valen,E. (2014) CHOPCHOP: a CRISPR/Cas9 and TALEN web tool for genome editing. *Nucleic Acids Res.*, **42**, W401–W407.
36. Trapnell,C., Pachter,L. and Salzberg,S.L. (2009) TopHat: discovering splice junctions with RNA-Seq. *Bioinformatics*, **25**, 1105–1111.
37. Anders,S., McCarthy,D.J., Chen,Y., Okoniewski,M., Smyth,G.K., Huber,W. and Robinson,M.D. (2013) Count-based differential expression analysis of RNA sequencing data using R and Bioconductor. *Nat. Protoc.*, **8**, 1765–1786.
38. Anders,S., Pyl,P.T. and Huber,W. (2015) HTSeq–a Python framework to work with high-throughput sequencing data. *Bioinformatics*, **31**, 166–169.
39. Love,M.I., Huber,W. and Anders,S. (2014) Moderated estimation of fold change and dispersion for RNA-seq data with DESeq2. *Genome Biol.*, **15**, 550.
40. Shen,S., Park,J.W., Huang,J., Dittmar,K.A., Lu,Z.X., Zhou,Q., Carstens,R.P. and Xing,Y. (2012) MATS: a Bayesian framework for flexible detection of differential alternative splicing from RNA-Seq data. *Nucleic Acids Res.*, **40**, e61.
41. Mockenhaupt,S. and Makeyev,E.V. (2015) Non-coding functions of alternative pre-mRNA splicing in development. *Semin. Cell Dev. Biol.*, **47–48**, 32–39.
42. Kozak,M. (2002) Pushing the limits of the scanning mechanism for initiation of translation. *Gene*, **299**, 1–34.
43. Durinck,S., Moreau,Y., Kasprzyk,A., Davis,S., De Moor,B., Brazma,A. and Huber,W. (2005) BioMart and Bioconductor: a powerful link between biological databases and microarray data analysis. *Bioinformatics*, **21**, 3439–3440.
44. Gao,Y., Zhang,Y., Zhang,D., Dai,X., Estelle,M. and Zhao,Y. (2015) Auxin binding protein 1 (ABP1) is not required for either auxin signaling or Arabidopsis development. *Proc. Natl. Acad. Sci. U.S.A.*, **112**, 2275–2280.
45. Yamamoto,S., Jaiswal,M., Charng,W.L., Gambin,T., Karaca,E., Mirzaa,G., Wiszniewski,W., Sandoval,H., Haelterman,N.A., Xiong,B. *et al.* (2014) A drosophila genetic resource of mutants to study mechanisms underlying human genetic diseases. *Cell*, **159**, 200–214.
46. De Souza,A.T., Dai,X., Spencer,A.G., Reppen,T., Menzie,A., Roesch,P.L., He,Y., Caguyong,M.J., Bloomer,S., Herweijer,H. *et al.* (2006) Transcriptional and phenotypic comparisons of Ppara knockout and siRNA knockdown mice. *Nucleic Acids Res.*, **34**, 4486–4494.
47. Ulitsky,I., Shkumatava,A., Jan,C.H., Sive,H. and Bartel,D.P. (2011) Conserved function of lincRNAs in vertebrate embryonic development despite rapid sequence evolution. *Cell*, **147**, 1537–1550.
48. Tsai,S.Q., Zheng,Z., Nguyen,N.T., Liebers,M., Topkar,V.V., Thapar,V., Wyvekens,N., Khayter,C., Iafrate,A.J., Le,L.P. *et al.* (2015) GUIDE-seq enables genome-wide profiling of off-target cleavage by CRISPR-Cas nucleases. *Nat. Biotechnol.*, **33**, 187–197.
49. Coffman,J.A., Dickey-Sims,C., Haug,J.S., McCarthy,J.J. and Robertson,A.J. (2004) Evaluation of developmental phenotypes produced by morpholino antisense targeting of a sea urchin Runx gene. *BMC Biol.*, **2**, 6.
50. Wahl,M.C., Will,C.L. and Luhrmann,R. (2009) The spliceosome: design principles of a dynamic RNP machine. *Cell*, **136**, 701–718.
51. Eisen,J.S. and Smith,J.C. (2008) Controlling morpholino experiments: don't stop making antisense. *Development*, **135**, 1735–1743.